Autonomous Orbit Determination of Multiple Spacecraft Using Active Sensing with Satellite-to-Satellite Tracking

By Kota KAKIHARA,[1)] Naoya OZAKI,[1)] and Ryu FUNASE[1)]

[1)]*Department of Aeronautics and Astronautics, The University of Tokyo, Tokyo, Japan*

Conventional ground-based orbit navigation systems are well-developed but expensive, and it is excessive for reasonable missions. Therefore, autonomous orbit determination without ground stations will be significant for future interplanetary missions. Satellite-to-satellite tracking (SST) is a measurement to observe the relative range between multiple spacecraft, and it is applicable for autonomous orbit determination. Previous studies show that orbits are observable by using only SST data if spacecraft is strongly perturbed by the third body, and this method cannot be applied to general problems because of the uncertainty of orbit orientations. This research proposes a new orbit navigation method using SST and active sensing technology. The proposed method uses more than two active sensing maneuvers and these maneuvers yield the information of the orientation. Three types of analyses, that is, 1) geometrical, 2) analytical, and 3) numerical analyses, prove that the positions and velocities of two spacecraft and the magnitudes of ΔVs are observable if there are at least two active sensing maneuvers and the information of orientations of ΔVs is given. Numerical simulations verify the proposed algorithm and indicate that the estimation errors depend on the orientations of ΔVs. This result shows that the proposed method will be practically applied to interplanetary missions.

Key Words: Active Sensing, Autonomous Orbit Determination, Satellite-to-Satellite Tracking

Nomenclature

t	:	time
a	:	semi-major axis
e	:	eccentricity
ν	:	true anomaly
i	:	inclination
Ω	:	longitude of ascending node
ω	:	argument of perigee
c, d	:	relative angle
μ	:	gravitational constant
σ	:	standard deviation of error
ρ	:	crosslink range
α, β	:	spacecraft's name
λ	:	parameter of ridge regression
$\hat{\boldsymbol{P}}$	:	basis vector of periapsis direction
$\hat{\boldsymbol{Q}}$	:	cross product of $\hat{\boldsymbol{R}}$ and $\hat{\boldsymbol{P}}$
$\hat{\boldsymbol{R}}$	:	basis vector parallel to angular momentum
$\boldsymbol{r}, r$	:	position vector and its norm
$\boldsymbol{v}$	:	velocity vector
$\Delta\boldsymbol{v}, \Delta\hat{\boldsymbol{v}}$	:	ΔV vector and its orientation
$\boldsymbol{X}$	:	state vector
$\boldsymbol{Y}$	:	observation vector
$\boldsymbol{x}$	:	linearized state vector
$\boldsymbol{y}$	:	linearized observation vector
$\boldsymbol{\epsilon}$	:	noise vector
Φ	:	state transition matrix
P	:	variance-covariance matrix
Superscripts		
$*$	:	reference
-	:	a priori
Subscripts		
$+$	:	after maneuver
$-$	:	before maneuver

1. Introduction

Autonomous orbit determination is one of the essential technologies for future interplanetary missions. Most deep space probes determine their orbit based on the Earth-based observations. However, ground resources get stringent with increasing the number of interplanetary missions. For interplanetary micro-spacecraft, especially, the orbit determination is a bottleneck for low-cost and frequent missions.

One of the promising ideas uses Satellite-to-Satellite Tracking (SST) between multiple spacecraft and determines their orbits in the inertial frame. Markley (1984) and Psiaki (1999) have studied the orbit determination using the measurement of relative range and angle of two spacecraft.[6)7)] For interplanetary missions, however, the relative angle cannot be measured if two spacecraft is distant from each other. Hill and Born (2007) have proposed liaison navigation, which uses only crosslink range of multiple spacecraft, and proven that their orbits can be completely determined in the inertial frame if the dynamics of the spacecraft is highly influenced by third body's gravity.[2)] However, the liaison navigation cannot determine the inertial orbits for general dynamical systems.[2)] This is because the orientation of the orbits is unobservable through the crosslink range, whereas the size and shape of them are observable.

This paper proposes a new autonomous orbit determination method in general dynamical systems. The proposed method uses only crosslink range information but determines the inertial orbits completely by applying the active sensing strategy. Active sensing is a technology to recover the observability by executing active maneuvers. For example, Woffinden and Geller (2009) analyses optimal active rendezvous maneuvers for angles-only navigation to determine the relative orbits.[10)] It is proven that the inertial orbits can be determined with crosslink range if the spacecraft executes more than two maneu-

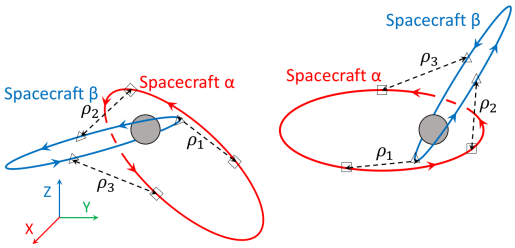

Fig. 1. Rotational symmetry about two-body problem.

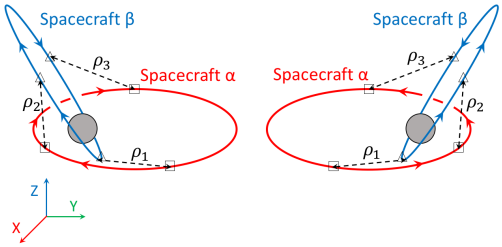

Fig. 2. Reflection symmetry about two-body problem.

vers. In this paper, the proposed method is verified with three ways: 1) geometrical approach, 2) theoretical approach, and 3) numerical approach. Finally, numerical examples present that the proposed algorithm is practical for deep space missions.

2. Orbit Determination by SST

Spacecraft orbits are observable when the orbits are uniquely determined. For example, in the two-body problem, two pairs of orbits in Fig. 1 cannot be distinguished from each other by SST observation because they coincide by rotational transformation and their range histories are the same. Pairs in Fig. 2 also cannot be distinguished because they coincide by reflection.

According to Hill and Born (2007), when the acceleration field and its time-derivative are symmetric, orbits are not unique and SST does not provide enough information for orbit determination.[2] In the two-body problem, there are rotational symmetry about the center of the primary body and reflection symmetry about any plane including that point. This is the reason orbits cannot be observable in the two-body problem.

Furthermore, Liu and Liu (2001) states that it is possible to determine the semi-major axis, the eccentricity, and the true anomaly of two spacecraft in the two-body problem by using SST only, but it is impossible to estimate the inclination, the longitude of the ascending node, and the argument of perigee of them.[5] However, Hill and Born (2007) showed relative orientation angles d, c_α, c_β, defined in Fig. 3, can be estimated.[2] These angles do not change by any rotation or reflection.

In the three-body problem, however, time derivative of acceleration field is not symmetric except for reflection symmetry about the ecliptic plane, and orbits can be determined by SST data.[2] This is because there are only two possible pairs of orbits when there is only a reflection symmetry about a plane, and these orbits can be distinguished by using a priori information

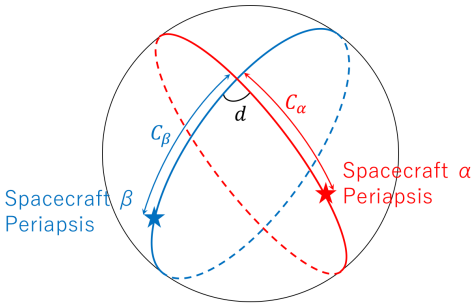

Fig. 3. Relative angles of two spacecraft orbits.

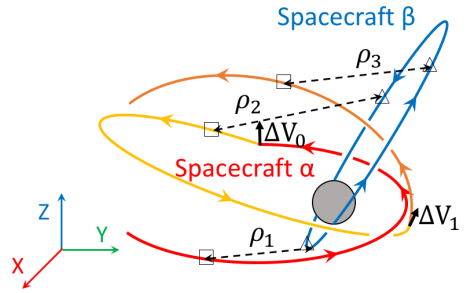

Fig. 4. Proposed method.

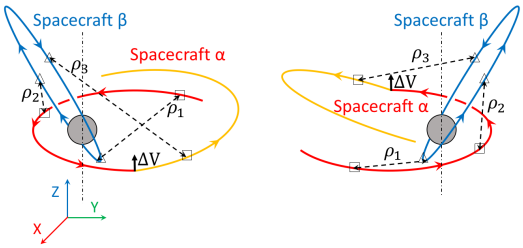

Fig. 5. Rotational symmetry about two-body problem with a maneuver.

about the orbits.

In the proposed method, ΔV maneuvers reduce symmetries of the two-body problem as shown in Fig. 4, and orbits can be estimated even in the two-body problem. These symmetries are discussed in the next section.

3. Geometrical Approach

In the two-body problem with ΔV maneuvers, the kinds of symmetries are variable depending on the number and the orientations of impulses. In the case of one maneuver, there is a rotational symmetry about an axis parallel to the ΔV vector passing through the center of the primary body as shown in Fig. 5. There is also a reflection symmetry about any plane including that axis. In this case, orbital elements about absolute orientation are not fully estimated because of the symmetries.

In the case of two ΔVs, if the two ΔV vectors are not parallel, there does not exist any rotational symmetry but there is a reflection symmetry about a plane including the center of the primary body and those two vectors. However, there are only two possible orbits like in the three-body problem, and these orbits also can be distinguished by a priori information. In the case of two maneuvers whose orientations are parallel, the situation is the same as the case of only one maneuver and orbital

elements cannot be fully estimated. There is no symmetry if there are more than three maneuvers whose ΔV vectors include three linearly independent vectors.

4. Analytical Approach

In this section, observability of the proposed method is analyzed by formulation. For the spacecraft α and β, let us determine the inertial orbits by SST with two impulsive maneuvers of the spacecraft α.

The position and the velocity of spacecraft are expressed with Keplerian elements, a, e, ν, and orbital basis vectors:

$$\boldsymbol{r} = \frac{a\left(1-e^2\right)}{1+e\cos\nu}\left(\cos\nu\hat{\boldsymbol{P}} + \sin\nu\hat{\boldsymbol{Q}}\right) \tag{1}$$

$$\boldsymbol{v} = \sqrt{\frac{\mu}{a\left(1-e^2\right)}}\left(-\sin\nu\hat{\boldsymbol{P}} + (e+\cos\nu)\,\hat{\boldsymbol{Q}}\right). \tag{2}$$

Therefore, it is necessary to determine a_α, a_β, e_α, e_β, ν_α, ν_β, $\hat{\boldsymbol{P}}_\alpha$, $\hat{\boldsymbol{P}}_\beta$, $\hat{\boldsymbol{Q}}_\alpha$, and $\hat{\boldsymbol{Q}}_\beta$ for orbit determination. As stated in Sec. **2.**, a_α, a_β, e_α, e_β, ν_α, and ν_β can be estimated by SST data only. Then, $\hat{\boldsymbol{P}}_\alpha$, $\hat{\boldsymbol{P}}_\beta$, $\hat{\boldsymbol{Q}}_\alpha$, and $\hat{\boldsymbol{Q}}_\beta$ should be determined by other calculations.

In the proposed method, the additional conditions to orbital basis vectors are the information of ΔVs. A ΔV vector is represented by Eq. (2) as follows.

$$\begin{aligned}\Delta\boldsymbol{v} &= \boldsymbol{v}_+ - \boldsymbol{v}_- \\ &= \sqrt{\frac{\mu}{a_{\alpha+}\left(1-e_{\alpha+}^2\right)}}\left(-\sin\nu_{\alpha+}\hat{\boldsymbol{P}}_{\alpha+} + (e_{\alpha+}+\cos\nu_{\alpha+})\,\hat{\boldsymbol{Q}}_{\alpha+}\right) \\ &- \sqrt{\frac{\mu}{a_{\alpha-}\left(1-e_{\alpha-}^2\right)}}\left(-\sin\nu_{\alpha-}\hat{\boldsymbol{P}}_{\alpha-} + (e_{\alpha-}+\cos\nu_{\alpha-})\,\hat{\boldsymbol{Q}}_{\alpha-}\right)\end{aligned} \tag{3}$$

In one ΔV case, let us consider a rotational transformation matrix Θ whose eigenvector corresponding to the eigenvalue 1 is $\Delta\boldsymbol{v}$. This matrix is applied to Eq. (3) and then

$$\begin{aligned}\Theta\Delta\boldsymbol{v} &= \Delta\boldsymbol{v} \\ &= \sqrt{\frac{\mu}{a_{\alpha+}\left(1-e_{\alpha+}^2\right)}}\left(-\sin\nu_{\alpha+}\Theta\hat{\boldsymbol{P}}_{\alpha+} + (e_{\alpha+}+\cos\nu_{\alpha+})\,\Theta\hat{\boldsymbol{Q}}_{\alpha+}\right) \\ &- \sqrt{\frac{\mu}{a_{\alpha-}\left(1-e_{\alpha-}^2\right)}}\left(-\sin\nu_{\alpha-}\Theta\hat{\boldsymbol{P}}_{\alpha-} + (e_{\alpha-}+\cos\nu_{\alpha-})\,\Theta\hat{\boldsymbol{Q}}_{\alpha-}\right).\end{aligned} \tag{4}$$

Eqs. (3) and (4) show that ($\hat{\boldsymbol{P}}_{\alpha+}$, $\hat{\boldsymbol{Q}}_{\alpha+}$, $\hat{\boldsymbol{P}}_{\alpha-}$, $\hat{\boldsymbol{Q}}_{\alpha-}$) and ($\Theta\hat{\boldsymbol{P}}_{\alpha+}$, $\Theta\hat{\boldsymbol{Q}}_{\alpha+}$, $\Theta\hat{\boldsymbol{P}}_{\alpha-}$, $\Theta\hat{\boldsymbol{Q}}_{\alpha-}$) cannot be distinguished by information of one ΔV only. This result corresponds to rotational symmetry stated in Sec. **3.**. Reflection symmetry is also shown similarly by considering a reflection transformation matrix whose eigenvector corresponding to the eigenvalue 1 is $\Delta\boldsymbol{v}$.

In two ΔVs case, dot products of $\Delta\hat{\boldsymbol{v}}$ and $\hat{\boldsymbol{P}}_\beta$, $\hat{\boldsymbol{Q}}_\beta$, $\hat{\boldsymbol{R}}_\beta$ are considered.

$$\Delta\hat{\boldsymbol{v}}\cdot\hat{\boldsymbol{P}}_\beta = \Delta\boldsymbol{v}\cdot\hat{\boldsymbol{P}}_\beta/\|\Delta\boldsymbol{v}\| \tag{5}$$

$$\Delta\hat{\boldsymbol{v}}\cdot\hat{\boldsymbol{Q}}_\beta = \Delta\boldsymbol{v}\cdot\hat{\boldsymbol{Q}}_\beta/\|\Delta\boldsymbol{v}\| \tag{6}$$

$$\Delta\hat{\boldsymbol{v}}\cdot\hat{\boldsymbol{R}}_\beta = \Delta\boldsymbol{v}\cdot\hat{\boldsymbol{R}}_\beta/\|\Delta\boldsymbol{v}\| \tag{7}$$

where $\Delta\hat{\boldsymbol{v}}$ and $\|\Delta\boldsymbol{v}\|$ are given. $\Delta\boldsymbol{v}\cdot\hat{\boldsymbol{P}}_\beta$, $\Delta\boldsymbol{v}\cdot\hat{\boldsymbol{Q}}_\beta$, and $\Delta\boldsymbol{v}\cdot\hat{\boldsymbol{R}}_\beta$ can be calculated from Eq. (3) if dot products between $\hat{\boldsymbol{P}}_\alpha$, $\hat{\boldsymbol{P}}_\beta$, $\hat{\boldsymbol{Q}}_\alpha$, $\hat{\boldsymbol{Q}}_\beta$, $\hat{\boldsymbol{R}}_\alpha$, and $\hat{\boldsymbol{R}}_\beta$ are known. As shown in the Appendix B, these values are the function of relative angles c_α, c_β, and d, which can be estimated in the two-body problem. Therefore, $\Delta\hat{\boldsymbol{v}}\cdot\hat{\boldsymbol{P}}_\beta$, $\Delta\hat{\boldsymbol{v}}\cdot\hat{\boldsymbol{Q}}_\beta$, and $\Delta\hat{\boldsymbol{v}}\cdot\hat{\boldsymbol{R}}_\beta$ can be calculated.

Then, $\hat{\boldsymbol{P}}_\beta$ and $\hat{\boldsymbol{Q}}_\beta$ are represented as follows if $\Delta\hat{\boldsymbol{v}}_0$ and $\Delta\hat{\boldsymbol{v}}_1$ are not parallel (see Appendix C).

$$\begin{aligned}\hat{\boldsymbol{P}}_\beta = {} & \frac{p-r\cos\theta}{1-\cos^2\theta}\Delta\hat{\boldsymbol{v}}_0 + \frac{-p\cos\theta+r}{1-\cos^2\theta}\Delta\hat{\boldsymbol{v}}_1 \\ & \pm\frac{\sqrt{2pr\cos\theta-p^2-r^2+1-\cos^2\theta}}{1-\cos^2\theta}\left(\Delta\hat{\boldsymbol{v}}_0\times\Delta\hat{\boldsymbol{v}}_1\right)\end{aligned} \tag{8}$$

$$\begin{aligned}\hat{\boldsymbol{Q}}_\beta = {} & \frac{q-s\cos\theta}{1-\cos^2\theta}\Delta\hat{\boldsymbol{v}}_0 + \frac{-q\cos\theta+s}{1-\cos^2\theta}\Delta\hat{\boldsymbol{v}}_1 \\ & \pm\frac{\sqrt{2qs\cos\theta-q^2-s^2+1-\cos^2\theta}}{1-\cos^2\theta}\left(\Delta\hat{\boldsymbol{v}}_0\times\Delta\hat{\boldsymbol{v}}_1\right)\end{aligned} \tag{9}$$

$$p = \Delta\hat{\boldsymbol{v}}_0\cdot\hat{\boldsymbol{P}}_\beta \tag{10}$$

$$q = \Delta\hat{\boldsymbol{v}}_0\cdot\hat{\boldsymbol{Q}}_\beta \tag{11}$$

$$r = \Delta\hat{\boldsymbol{v}}_1\cdot\hat{\boldsymbol{P}}_\beta \tag{12}$$

$$s = \Delta\hat{\boldsymbol{v}}_1\cdot\hat{\boldsymbol{Q}}_\beta \tag{13}$$

$$\cos\theta = \Delta\hat{\boldsymbol{v}}_0\cdot\Delta\hat{\boldsymbol{v}}_1 \tag{14}$$

The plus-minus signs show reflection symmetry as stated in Sec. **3.**. There are four combinations of plus-minus signs in Eqs. (8) and (9), but there is a constraint

$$\hat{\boldsymbol{P}}_\beta\cdot\hat{\boldsymbol{Q}}_\beta = 0, \tag{15}$$

and the number of possible combinations is reduced to two by this constraint. Therefore, $\hat{\boldsymbol{P}}_\beta$ and $\hat{\boldsymbol{Q}}_\beta$ can be determined if there is a priori information as stated in Sec. **3.**. $\hat{\boldsymbol{P}}_\alpha$ and $\hat{\boldsymbol{Q}}_\alpha$ are calculated from dot products of orbital basis vectors shown in Appendix B after $\hat{\boldsymbol{P}}_\beta$ and $\hat{\boldsymbol{Q}}_\beta$ are determined.

Additionally, $\|\Delta\boldsymbol{v}\|$ can be calculated as follows.

$$\|\Delta\boldsymbol{v}\| = \sqrt{\left(\Delta\boldsymbol{v}\cdot\hat{\boldsymbol{P}}_\beta\right)^2 + \left(\Delta\boldsymbol{v}\cdot\hat{\boldsymbol{Q}}_\beta\right)^2 + \left(\Delta\boldsymbol{v}\cdot\hat{\boldsymbol{R}}_\beta\right)^2} \tag{16}$$

Therefore, only information of $\Delta\hat{\boldsymbol{v}}$ and a priori information of orbits are needed for orbit determination by the proposed method.

5. Numerical Approach

In this section, the numerical approach demonstrates that the proposed algorithm can determine a pair of orbits in the inertial frame. The numerical simulations consider that two spacecraft α and β, the spacecraft α executes orbital maneuvers, and compare the results.

5.1. Estimation Algorithm

This simulations use the batch processor algorithm shown in Ref. 8) with some modifications. For the state vector

$$\boldsymbol{X} = \left[\begin{array}{ccccccc}\boldsymbol{r}_\alpha^T & \boldsymbol{v}_\alpha^T & \boldsymbol{r}_\beta^T & \boldsymbol{v}_\beta^T & \|\Delta\boldsymbol{v}_0\| & \|\Delta\boldsymbol{v}_1\|\end{array}\right]^T, \tag{17}$$

and the observation vector

$$\boldsymbol{Y}_i = \rho_i, \tag{18}$$

the state and observation equation are as follows.

$$\dot{\boldsymbol{X}} = \boldsymbol{F}(\boldsymbol{X}) \tag{19}$$

$$= \begin{bmatrix} \boldsymbol{v}_\alpha^T & -\frac{\mu}{r_\alpha^3}\boldsymbol{r}_\alpha^T & \boldsymbol{v}_\beta^T & -\frac{\mu}{r_\beta^3}\boldsymbol{r}_\beta^T & 0 & 0 \end{bmatrix}^T \tag{20}$$

$$\boldsymbol{Y}_i = \boldsymbol{G}(\boldsymbol{X}_i) + \boldsymbol{\epsilon}_i \tag{21}$$

$$= \|\boldsymbol{r}_{\alpha i} - \boldsymbol{r}_{\beta i}\| + \boldsymbol{\epsilon}_i \tag{22}$$

where the subscript i represents the epoch of the observation.

These equations are linearized around the reference orbit $\boldsymbol{X}^*$ and $\boldsymbol{Y}^*$. The linearized state and observation vectors are

$$\boldsymbol{x} = \boldsymbol{X} - \boldsymbol{X}^*,\ \boldsymbol{y} = \boldsymbol{Y} - \boldsymbol{Y}^*. \tag{23}$$

Therefore the linearized equations are expressed with the linearized state and observation vectors:

$$\dot{\boldsymbol{x}} = A\boldsymbol{x} \tag{24}$$

$$\boldsymbol{y}_i = \tilde{H}_i\boldsymbol{x}_i + \boldsymbol{\epsilon}_i \tag{25}$$

$$A = \left[\frac{\partial \boldsymbol{F}}{\partial \boldsymbol{X}}\right]^*,\ \tilde{H}_i = \left[\frac{\partial \boldsymbol{G}}{\partial \boldsymbol{X}}\right]_i^* \tag{26}$$

where we neglect the higher order terms of the Taylor series expansions of $\boldsymbol{F}(\boldsymbol{X})$ and $\boldsymbol{G}(\boldsymbol{X}_i)$.

The state vector $\boldsymbol{x}_k$ at epoch t_k is expressed with a state transition matrix (STM) and the state vector at an initial epoch.

$$\boldsymbol{x}_k = \Phi(t_k, t_0)\boldsymbol{x}_0 \tag{27}$$

The STM is computed by integrating the following ordinary differential equation.

$$\dot{\Phi}(t_k, t_0) = A_k\Phi(t_k, t_0) \tag{28}$$

where the initial condition is $\Phi(t_0, t_0) = I$. The effects of impulsive maneuvers are included to the STM (Appendix D).

When we have multiple observations $\boldsymbol{y}_1, \boldsymbol{y}_2, ...\boldsymbol{y}_l$, the observation vectors and observation equation are expressed with the state vector $\boldsymbol{x}_0$ at the initial epoch and the STM.

$$\boldsymbol{y} = H\boldsymbol{x}_0 + \boldsymbol{\epsilon} \tag{29}$$

$$\boldsymbol{y} = \begin{bmatrix} \boldsymbol{y}_1 \\ \vdots \\ \boldsymbol{y}_l \end{bmatrix},\ H = \begin{bmatrix} \tilde{H}_1\Phi(t_1, t_0) \\ \vdots \\ \tilde{H}_l\Phi(t_l, t_0) \end{bmatrix}\ \boldsymbol{\epsilon} = \begin{bmatrix} \boldsymbol{\epsilon}_1 \\ \vdots \\ \boldsymbol{\epsilon}_l \end{bmatrix} \tag{30}$$

The minimum variance estimation of the initial state vector is

$$\boldsymbol{x}_{0est} = \left(H^T W H\right)^{-1}\left(H^T W \boldsymbol{y}\right) \tag{31}$$

$$W_i = \frac{1}{\sigma^2} \tag{32}$$

where $\boldsymbol{x}_{0est}$ is the maximum likelihood state vector. For solving nonlinear problems, we expand the nonlinear state and observation equations around the updated reference orbits ($\boldsymbol{X}_0^* + \boldsymbol{x}_{0est}$), solve the minimum variance estimation, and continue these processes iteratively until the orbits converge.

In this study, the estimation algorithm is modified because it is not robust to linearization errors and the iteration may diverge. The modified algorithm minimizes the objective function

$$J(\boldsymbol{x}_0) = \sum_i \phi(\boldsymbol{y}_i - H_i\boldsymbol{x}_0) + 1/2\lambda\boldsymbol{x}_0^T\boldsymbol{x}_0 \tag{33}$$

$$\phi(u) = \begin{cases} \frac{1}{2\sigma^2}u^2 & (|u| < C) \\ \frac{1}{\sigma^2}C(|u| - 1/2C) & (otherwise). \end{cases} \tag{34}$$

Table 1. Simulation parameter settings.

$\boldsymbol{r}_{\alpha 0}$	$\left[4{\times}10^3,\ 0,\ 0\right]^T$	km
$\boldsymbol{v}_{\alpha 0}$	$[0,\ 3600,\ 0]^T$	m/s
$\boldsymbol{r}_{\beta 0}$	$\left[4.5{\times}10^3,\ 4.5{\times}10^3,\ 0\right]^T$	km
$\boldsymbol{v}_{\beta 0}$	$[-800,\ 900,\ 2000]^T$	m/s
$\|\Delta\boldsymbol{v}_0\|$	10.0749	m/s
$\|\Delta\boldsymbol{v}_1\|$	10.1694	m/s
primary body	Mars	-
t_{oi}	10	s
$\Delta\hat{\boldsymbol{v}}_0$	$[0,\ 0.866,\ 0.5]^T$	-
$\Delta\hat{\boldsymbol{v}}_1$	$[-0.6061,\ 0.6061,\ -0.5152]^T$	-
σ	10	m

Table 2. Estimation parameter settings.

$\overline{\boldsymbol{r}_{\alpha 0}}$	$\left[3.8{\times}10^3,\ -1{\times}10^2,\ -7{\times}10^2\right]^T$	km
$\overline{\boldsymbol{v}_{\alpha 0}}$	$[100,\ 3500,\ -400]^T$	m/s
$\overline{\boldsymbol{r}_{\beta 0}}$	$\left[4.5{\times}10^3,\ 4{\times}10^3,\ 2.4{\times}10^3\right]^T$	km
$\overline{\boldsymbol{v}_{\beta 0}}$	$[-1200,\ 400,\ 1800]^T$	m/s
$\overline{\|\Delta\boldsymbol{v}_0\|}$	10	m/s
$\overline{\|\Delta\boldsymbol{v}_1\|}$	10	m/s
C	100	m

The first term is the same as Huber's robust minimum least squares method.[4] The second term is used for ridge regression.[3]

The estimation algorithm is summarized as follows.

1. Reference orbit (RO), $\boldsymbol{X}^*$ and $\boldsymbol{Y}_i^*$, is generated by using a priori information($\overline{\boldsymbol{X}_0}$).
2. $\overline{\boldsymbol{x}}_0$, $\boldsymbol{y}_i$, $\Phi(t, t_0)$, $\tilde{H}_i$ are calculated with RO.
3. The maximum likelihood state vector $\boldsymbol{x}_{0est}$ is estimated by

$$\boldsymbol{x}_{0est} = P_0\left(H^T W \boldsymbol{y}\right) \tag{35}$$

$$P_0 = \left(\lambda I + H^T W H\right)^{-1} \tag{36}$$

$$W_i = \begin{cases} \frac{1}{\sigma^2} & (\|\boldsymbol{y}_i\| < C) \\ \frac{C}{\sigma^2\|\boldsymbol{y}_i\|} & (otherwise). \end{cases} \tag{37}$$

4. The reference orbit is updated as $\boldsymbol{X}_0^* \leftarrow \boldsymbol{X}_0^* + \boldsymbol{x}_{0est}$. If $\boldsymbol{x}_{0est}$ is smaller than a specified value, λ is decreased. The iteration ends if λ converges to zero. Otherwise, the procedure returns to 2.

5.2. Parameter Settings

The simulation parameters are shown in Tables 1 and 2 where t_{oi} is the observation interval. The total observation time is 14400 s and the maneuver execution time is 7200 s for one ΔV case and 4800 s and 9600 s for two ΔVs case. The execution error of $\Delta\hat{\boldsymbol{v}}$ and the visibility of range measurement is not considered in these simulations.

5.3. Results and Discussion

The results are shown in Figs. 6, 7, and 8. In these figures, the shape and size of the estimated orbits become the same as those of the true orbits in all cases. However, the orientations of the estimated orbits do not coincide with those of the true orbits in ballistic and one ΔV cases, and the estimated orbits converge to the true orbits in two ΔVs case. In one ΔV case, the rotational axis between the true and estimated orbits is parallel to the ΔV vector.

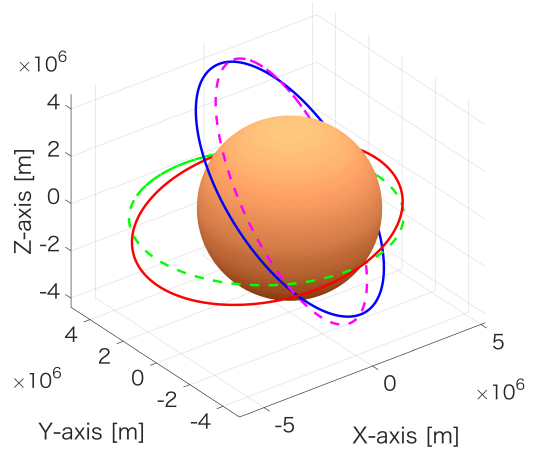

Fig. 6. True orbits and estimated orbits in no ΔV case. The green and magenta dashed orbits are true orbits of α and β. The red and blue represent estimated orbits of α and β respectively.

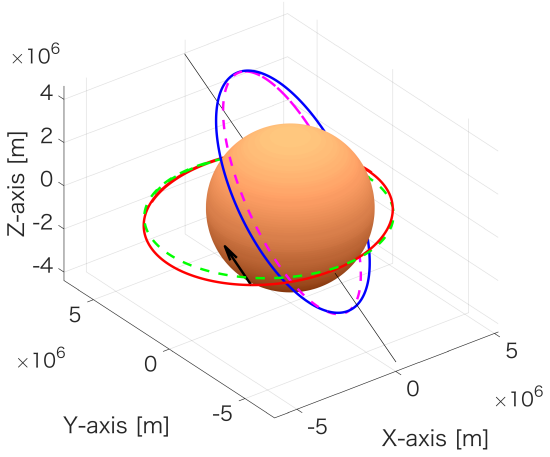

Fig. 7. True orbits and estimated orbits in one ΔV case. The black line is the axis of rotation between true orbits and estimated orbits. The allow represents ΔV vector.

The result of the estimation in two ΔVs case is as follows.

$$\boldsymbol{r}_{\alpha 0 est} - \boldsymbol{r}_{\alpha 0} = [10,\ 5552,\ -2851]^T \text{ m} \quad (38)$$

$$\boldsymbol{v}_{\alpha 0 est} - \boldsymbol{v}_{\alpha 0} = [-5.00,\ -0.01,\ 2.08]^T \text{ m/s} \quad (39)$$

$$\boldsymbol{r}_{\beta 0 est} - \boldsymbol{r}_{\beta 0} = [-6251, 6243,\ -609]^T \text{ m} \quad (40)$$

$$\boldsymbol{v}_{\beta 0 est} - \boldsymbol{v}_{\beta 0} = [0.18,\ -2.27,\ 1.09]^T \text{ m/s} \quad (41)$$

$$\|\Delta \boldsymbol{v_0}\|_{est} - \|\Delta \boldsymbol{v_0}\| = -0.0034 \text{m/s} \quad (42)$$

$$\|\Delta \boldsymbol{v_1}\|_{est} - \|\Delta \boldsymbol{v_1}\| = 0.0037 \text{m/s} \quad (43)$$

$$\sqrt{\max \text{eig}\,(P_{0r\alpha})} = 5.09 \text{ km} \quad (44)$$

$$\sqrt{\max \text{eig}\,(P_{0v\alpha})} = 3.51 \text{ m/s} \quad (45)$$

$$\sqrt{\max \text{eig}\left(P_{0r\beta}\right)} = 7.15 \text{ km} \quad (46)$$

$$\sqrt{\max \text{eig}\left(P_{0v\beta}\right)} = 2.49 \text{ m/s} \quad (47)$$

where $\sqrt{\max \text{eig}\,(P)}$ means the square root of the maximum eigenvalue of the covariance matrix P and its subscript represents the corresponding portion of it.

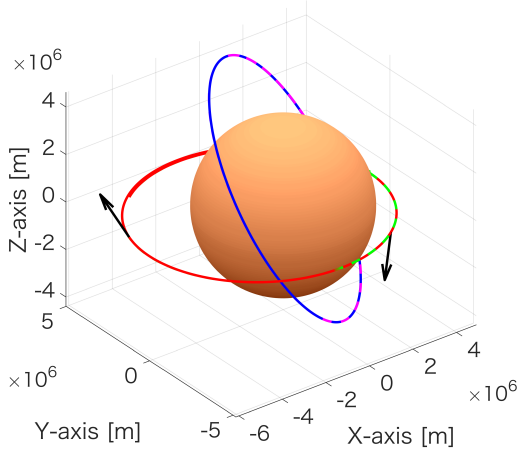

Fig. 8. True orbits and estimated orbits in two ΔVs case.

The result shows that the orbits and the magnitude of ΔVs can be estimated with higher precision than a priori information. Finally, these numerical results demonstrate the orbit determination with active sensing in the two-body problems.

6. Estimation Considering Error of Δv

This section considers more realistic situations by discussing the numerical simulation and its estimation result when the magnitude and direction errors of $\Delta \boldsymbol{v}$ are not negligible. The simulation is conducted under the almost same condition as Sec. **5.2.**. The difference is that the ΔV errors are considered and the magnitudes of $\Delta \boldsymbol{v}$ are not estimated. However, the errors of ΔV magnitudes and orientations are regarded as consider parameters and the covariance matrix was calculated including these errors.

6.1. Maneuver Execution Error Model

Gates model is adopted as the maneuver execution error model.[1] The execution error is represented as normal distribution whose mean is zero and variance is formulated as follows.

$$\sigma_m^2 = \sigma_{mfixed}^2 + \sigma_{mprop}^2 \overline{\|\Delta \boldsymbol{v}\|}^2 \quad (48)$$

$$\sigma_o^2 = \sigma_{ofixed}^2 + \sigma_{oprop}^2 \overline{\|\Delta \boldsymbol{v}\|}^2 \quad (49)$$

where σ_m^2 is a variance along $\Delta \hat{\boldsymbol{v}}$ and σ_o^2 is variance in the plane normal to $\Delta \hat{\boldsymbol{v}}$. These variances consist of fixed errors and proportional errors.

6.2. Parameter Settings

The different parameters from Sec. **5.2.** are shown in Table 3. The 1996 pre-launch model of Cassini-Huygens's Main Engine Assembly is used for the values of Gates execution error model.[9]

6.3. Result

Figure 9 shows the estimated orbits and the true orbits. We realize that these orbits are very close each other. The differences between estimated and true state vectors and standard de-

Table 3. Simulation and Estimation parameter settings.

σ_{mfixed}	0.01	m/s
σ_{mprop}	0.35	%
σ_{ofixed}	0.0175	m/s
σ_{oprop}	10	mrad
$\|\Delta\boldsymbol{v}_0\|$	10.1	m/s
$\|\Delta\boldsymbol{v}_1\|$	9.9642	m/s
$\overline{\|\Delta\boldsymbol{v}_0\|}$	10	m/s
$\overline{\|\Delta\boldsymbol{v}_1\|}$	10	m/s
$\Delta\hat{\boldsymbol{v}}_0$	$[-0.0086,\ 0.8609,\ 0.5086]^T$	-
$\Delta\hat{\boldsymbol{v}}_1$	$[-0.6178,\ 0.6339,\ -0.4653]^T$	-
$\overline{\Delta\hat{\boldsymbol{v}}_0}$	$[0,\ 0.866,\ 0.5]^T$	-
$\overline{\Delta\hat{\boldsymbol{v}}_1}$	$[-0.6247,\ 0.6247,\ -0.4685]^T$	-

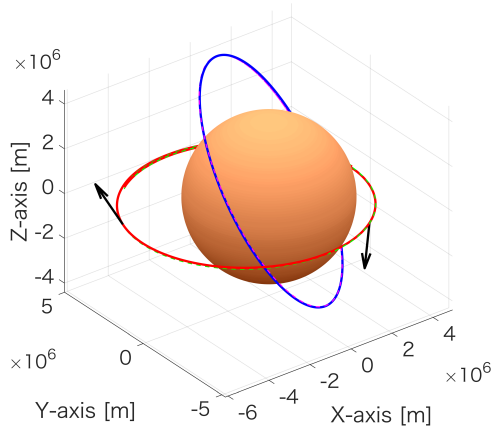

Fig. 9. True orbits and estimated orbits with two ΔVs considering $\Delta\hat{\boldsymbol{v}}$ errors.

viations are as follows.

$$\boldsymbol{r}_{\alpha 0est} - \boldsymbol{r}_{\alpha 0} = [-736,\ -65162,\ -34504]^T \text{ m} \quad (50)$$

$$\boldsymbol{v}_{\alpha 0est} - \boldsymbol{v}_{\alpha 0} = [58.63,\ -0.48,\ -12.49]^T \text{ m/s} \quad (51)$$

$$\boldsymbol{r}_{\beta 0est} - \boldsymbol{r}_{\beta 0} = [72432,\ -73932,\ -54414]^T \text{ m} \quad (52)$$

$$\boldsymbol{v}_{\beta 0est} - \boldsymbol{v}_{\beta 0} = [32.15,\ 19.54,\ 3.70]^T \text{ m/s} \quad (53)$$

$$\sqrt{\max \text{eig}\,(P_{0r\alpha})} = 91.9 \text{ km} \quad (54)$$

$$\sqrt{\max \text{eig}\,(P_{0v\alpha})} = 65.5 \text{ m/s} \quad (55)$$

$$\sqrt{\max \text{eig}\left(P_{0r\beta}\right)} = 121 \text{ km} \quad (56)$$

$$\sqrt{\max \text{eig}\left(P_{0v\beta}\right)} = 42.9 \text{ m/s} \quad (57)$$

The results are worse than the result without ΔV execution errors in Sec. **5.**, but the order of the errors is practical for some missions. Therefore, this method is also effective for orbit determination in the two-body problems even when execution errors of ΔVs are considered.

7. Sensitivity Analysis of ΔV Orientation

The estimation errors by the proposed algorithm depend on the orbital configurations of two spacecraft and timing/direction/magnitude of the orbital maneuvers. This section analyze the influence of ΔV direction on the estimation errors. Let us consider the influence of $\Delta\hat{\boldsymbol{v}}_2$ for a given $\Delta\hat{\boldsymbol{v}}_1$.

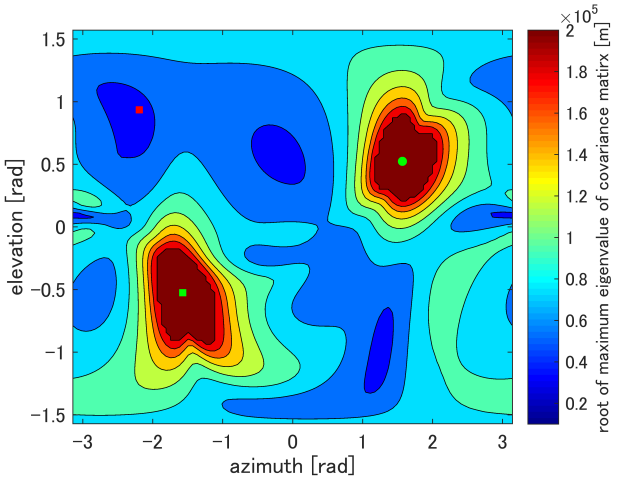

Fig. 10. Relationship between $\Delta\hat{\boldsymbol{v}}_1$ and $\sqrt{\max \text{eig}\,(P_{0r\alpha})}$. Green circle and square represent $\Delta\hat{\boldsymbol{v}}_0$ and $-\Delta\hat{\boldsymbol{v}}_0$ respectively. Red square is placed on $\Delta\hat{\boldsymbol{v}}_1$ which minimizes $\sqrt{\max \text{eig}\,(P_{0r\alpha})}$.

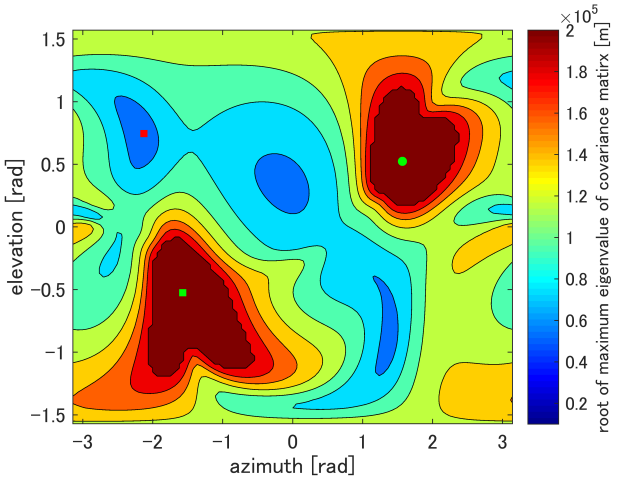

Fig. 11. Relationship between $\Delta\hat{\boldsymbol{v}}_1$ and $\sqrt{\max \text{eig}\left(P_{0r\beta}\right)}$.

$\sqrt{\max \text{eig}\,(P_{0r\alpha})}$ and $\sqrt{\max \text{eig}\left(P_{0r\beta}\right)}$ are used as the criteria to evaluate the determination errors, and these values are calculated for various $\Delta\hat{\boldsymbol{v}}_1$. P_0 is computed along true orbits because estimated orbits are near to them and P_{0true} is a good approximation of P_0 if estimation converges. The execution errors of ΔVs are also considered in this analysis. The simulation parameters are almost the same in Table 3., but $\|\Delta\boldsymbol{v}_0\|$ is 10m/s and $\Delta\hat{\boldsymbol{v}}_0$ is $[0,\ 0.866,\ 0.5]^T$.

Figures 10 and 11 show the maximum eigenvalue of the covariance matrices of the spacecraft α and β, respectively. These results indicate that $\Delta\hat{\boldsymbol{v}}_1$ affects the both covariance matrices. Therefore, an appropriate $\Delta\hat{\boldsymbol{v}}_1$ reduces the error of estimation and the optimal $\Delta\hat{\boldsymbol{v}}_1$ should be selected when the proposed method are conducted.

8. Conclusion

For autonomous orbit determination in interplanetary missions, various methods have been proposed. One of the sophisticated work uses Satellite-to-Satellite Tracking (SST) between multiple spacecraft and it can determine the spacecraft orbits in the inertial frame when the dynamical system is highly affected

by three-body perturbations. However, this method cannot be applied for general problems, such as two-body problems because of the orbital symmetries. This study proposes a new orbit navigation method using active sensing maneuvers and SST, and it can determine the spacecraft orbits completely in the inertial frame.

The observability of the proposed method is verified by geometrical, analytical and numerical approaches. These analyses show that orbits are observable in general problems, i.e. two-body problems, with active sensing maneuvers and at least two orbital maneuvers are necessary for the complete observability. In addition, the sensitivity analysis of the ΔV direction of the active sensing maneuvers shows that the ΔV directions have influence on the navigation errors, and there is an optimal direction to decrease the estimation errors.

The results show that the proposed method has potential to provide autonomous orbit determination strategy for interplanetary micro spacecraft which does not depend on ground stations. Further work will find the optimal ΔV direction to improve the estimation accuracy.

Acknowledgments

This research is supported by Shinichi Nakasuka, Ryu Funase, and Naoya Ozaki of The University of Tokyo and it would not have been possible without their advice.

Appendix**A** Orbital Basis Vectors

Orbital basis vectors, $\hat{\boldsymbol{P}}$, $\hat{\boldsymbol{Q}}$, $\hat{\boldsymbol{R}}$, are represented by Keplerian elements about orientations, i, Ω, ω, as follows.

$$\hat{\boldsymbol{P}} = \begin{bmatrix} \cos\omega\cos\Omega - \sin\omega\sin\Omega\cos i \\ \cos\omega\sin\Omega + \sin\omega\cos\Omega\cos i \\ \sin\omega\sin i \end{bmatrix} \tag{58}$$

$$\hat{\boldsymbol{Q}} = \begin{bmatrix} -\sin\omega\cos\Omega - \cos\omega\sin\Omega\cos i \\ -\sin\omega\sin\Omega + \cos\omega\cos\Omega\cos i \\ \cos\omega\sin i \end{bmatrix} \tag{59}$$

$$\hat{\boldsymbol{R}} = \hat{\boldsymbol{P}} \times \hat{\boldsymbol{Q}} = \begin{bmatrix} \sin\Omega\sin i \\ -\cos\Omega\sin i \\ \cos i \end{bmatrix} \tag{60}$$

Appendix**B** Relative Angles and Orbital Basis Vectors

The relationship between orbital basis vectors and relative angles are

$$\hat{\boldsymbol{P}}_\alpha \cdot \hat{\boldsymbol{P}}_\beta = \cos c_\alpha \cos c_\beta + \sin c_\alpha \sin c_\beta \cos d \tag{61}$$
$$\hat{\boldsymbol{P}}_\alpha \cdot \hat{\boldsymbol{Q}}_\beta = \cos c_\alpha \sin c_\beta - \sin c_\alpha \cos c_\beta \cos d \tag{62}$$
$$\hat{\boldsymbol{P}}_\alpha \cdot \hat{\boldsymbol{R}}_\beta = \mp \sin c_\alpha \sin d \tag{63}$$
$$\hat{\boldsymbol{Q}}_\alpha \cdot \hat{\boldsymbol{P}}_\beta = \sin c_\alpha \cos c_\beta - \cos c_\alpha \sin c_\beta \cos d \tag{64}$$
$$\hat{\boldsymbol{Q}}_\alpha \cdot \hat{\boldsymbol{Q}}_\beta = \sin c_\alpha \sin c_\beta + \cos c_\alpha \cos c_\beta \cos d \tag{65}$$
$$\hat{\boldsymbol{Q}}_\alpha \cdot \hat{\boldsymbol{R}}_\beta = \pm \cos c_\alpha \sin d \tag{66}$$
$$\hat{\boldsymbol{R}}_\alpha \cdot \hat{\boldsymbol{P}}_\beta = \pm \sin c_\beta \sin d \tag{67}$$
$$\hat{\boldsymbol{R}}_\alpha \cdot \hat{\boldsymbol{Q}}_\beta = \mp \cos c_\beta \sin d \tag{68}$$
$$\hat{\boldsymbol{R}}_\alpha \cdot \hat{\boldsymbol{R}}_\beta = \cos d. \tag{69}$$

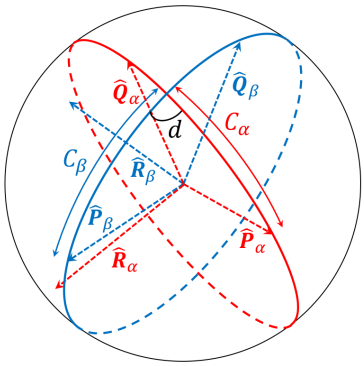

Fig. 12. Relative angles and orbital basis vectors.

These equations are derived by the spherical law of cosines in Fig. 12. The plus-minus signs are used because $\hat{\boldsymbol{R}}$ is a pseudo-vector and the sign of it is flipped by reflection.

Appendix**C** Relationship between $\hat{\boldsymbol{P}}_\beta$, $\hat{\boldsymbol{Q}}_\beta$ and ΔV Vectors

In two ΔVs case, $\hat{\boldsymbol{P}}_\beta$ and $\hat{\boldsymbol{Q}}_\beta$ is represented by $\Delta\hat{\boldsymbol{v}}_0$, $\Delta\hat{\boldsymbol{v}}_1$, and $\Delta\hat{\boldsymbol{v}}_0 \times \Delta\hat{\boldsymbol{v}}_1$ if $\Delta\hat{\boldsymbol{v}}_0$ and $\Delta\hat{\boldsymbol{v}}_1$ are not parallel.

$$\hat{\boldsymbol{P}}_\beta = l_p\Delta\hat{\boldsymbol{v}}_0 + m_p\Delta\hat{\boldsymbol{v}}_1 + n_p\Delta\hat{\boldsymbol{v}}_0 \times \Delta\hat{\boldsymbol{v}}_1 \tag{70}$$
$$\hat{\boldsymbol{Q}}_\beta = l_q\Delta\hat{\boldsymbol{v}}_0 + m_q\Delta\hat{\boldsymbol{v}}_1 + n_q\Delta\hat{\boldsymbol{v}}_0 \times \Delta\hat{\boldsymbol{v}}_1 \tag{71}$$

Therefore, dot products of $\Delta\hat{\boldsymbol{v}}_0$, $\Delta\hat{\boldsymbol{v}}_1$, $\hat{\boldsymbol{P}}_\beta$, and $\hat{\boldsymbol{Q}}_\beta$ are

$$p = \Delta\hat{\boldsymbol{v}}_0 \cdot \hat{\boldsymbol{P}}_\beta = l_p + m_p\cos\theta \tag{72}$$
$$q = \Delta\hat{\boldsymbol{v}}_0 \cdot \hat{\boldsymbol{Q}}_\beta = l_q + m_q\cos\theta \tag{73}$$
$$r = \Delta\hat{\boldsymbol{v}}_1 \cdot \hat{\boldsymbol{P}}_\beta = l_p\cos\theta + m_p \tag{74}$$
$$s = \Delta\hat{\boldsymbol{v}}_1 \cdot \hat{\boldsymbol{Q}}_\beta = l_q\cos\theta + m_q \tag{75}$$

where

$$\cos\theta = \Delta\hat{\boldsymbol{v}}_0 \cdot \Delta\hat{\boldsymbol{v}}_1 \tag{76}$$
$$\Delta\hat{\boldsymbol{v}}_0 \cdot (\Delta\hat{\boldsymbol{v}}_0\Delta \times \hat{\boldsymbol{v}}_1) = \Delta\hat{\boldsymbol{v}}_1 \cdot (\Delta\hat{\boldsymbol{v}}_0\Delta \times \hat{\boldsymbol{v}}_1) = 0. \tag{77}$$

These equations can be solved as follows.

$$l_p = \frac{p - r\cos\theta}{1 - \cos^2\theta} \tag{78}$$
$$m_p = \frac{-p\cos\theta + r}{1 - \cos^2\theta} \tag{79}$$
$$l_q = \frac{q - s\cos\theta}{1 - \cos^2\theta} \tag{80}$$
$$m_q = \frac{-q\cos\theta + s}{1 - \cos^2\theta} \tag{81}$$

n_p and n_q are derived from

$$\|\hat{\boldsymbol{P}}_\beta\|^2 = l_p^2 + m_p^2 + n_p^2\left(1 - \cos^2\theta\right) + 2l_pm_p\cos\theta = 1 \tag{82}$$
$$\|\hat{\boldsymbol{Q}}_\beta\|^2 = l_q^2 + m_q^2 + n_q^2\left(1 - \cos^2\theta\right) + 2l_qm_q\cos\theta = 1 \tag{83}$$

and solved as

$$n_p = \pm\frac{\sqrt{2pr\cos\theta - p^2 - r^2 + 1 - \cos^2\theta}}{1 - \cos^2\theta} \tag{84}$$
$$n_q = \pm\frac{\sqrt{2qs\cos\theta - q^2 - s^2 + 1 - \cos^2\theta}}{1 - \cos^2\theta}. \tag{85}$$

Appendix D STM considering ΔVs

The STM is defined as

$$\Phi(t_k, t_0) = \frac{\partial X_k}{\partial X_0}. \tag{86}$$

Then, the effect of ΔVs can be included by initializing the portion of STM about $\boldsymbol{v}_\alpha$ and $||\Delta \boldsymbol{v}||$ while integration of the STM.

$$\Phi(t_1, t_0)[4:6, 13] = \frac{\partial \boldsymbol{v}_{\alpha 1+}}{\partial ||\Delta \boldsymbol{v}_0||} = \Delta \hat{\boldsymbol{v}}_0 \tag{87}$$

$$\Phi(t_2, t_0)[4:6, 14] = \frac{\partial \boldsymbol{v}_{\alpha 2+}}{\partial ||\Delta \boldsymbol{v}_1||} = \Delta \hat{\boldsymbol{v}}_1 \tag{88}$$

References

1) Gates, C. R., "A Simplified Model of Midcourse Maneuver Execution Errors," Tech. Rep. 32-504, JPL, Pasadena, CA, October 15, 1963.
2) Hill, K., and Born, G. H., "Autonomous Interplanetary Orbit Determination Using Satellite-to-Satellite Tracking," *Journal of Guidance, Control, and Dynamics*, Vol. 30, No. 3, May-June 2007, pp. 679-686.
3) Hoerl, A. E., and R. W. Kennard. "Ridge Regression: Biased Estimation for Nonorthogonal Problems," *Technometrics*. Vol. 12, No. 1, 1970, pp. 5567.
4) Huber, P. J., "Robust estimation of a location parameter," *The Annals of Mathematical Statistics*, Vol. 35, No. 1, 1964, pp. 73-101.
5) Liu, Y., and Liu, L., "Orbit Determination Using Satellite-to-Satellite Tracking Data," *Chinese Journal of Astronomy and Astrophysics*, Vol. 1, No. 3, 2001, pp. 281-286.
6) Markley, F. L., "Autonomous Navigation Using Landmark and Intersatellite Data," *AIAA/AAS Astrodynamics Conference*, Seattle, WA, AIAA Paper 1984-1987, Aug. 1984.
7) Psiaki, M. L., "Autonomous Orbit Determination for Two Spacecraft from Relative Position Measurements," *Journal of Guidance, Control, and Dynamics*, Vol. 22, No. 2, March-April 1999, pp. 305-312.
8) Tapley, B. D., Schutz, B. E., and Born, G. H., *Statistical Orbit Determination*, Elsevier Academic Press, Burlington, MA, 2004.
9) Wagner, S. V., and Goodson, T. D., "Execution-Error Modeling and Analysis of the Cassini-Huygens Spacecraft Through 2007," AAS/AIAA Space Flight Mechanics Meeting, Galveston, TX, No. AAS 08-113, January 2008.
10) Woffinden, D. C., and Geller, D. K., "Optimal Orbital Rendezvous Maneuvering for Angles-Only Navigation," *Journal of Guidance, Control, and Dynamics*, Vol.32, No.4, 2009, pp.1382-1387.